# Fermi surface of field-induced ferromagnetic CeSb

M. R. Norman and D. D. Koelling

*Materials Science and Technology Division, Argonne National Laboratory, Argonne, Illinois 60439*

The Fermi surface of ferromagnetic CeSb is analyzed with use of a model in which the $f$ electrons in the system are treated as localized (unhybridized) $j = \frac{5}{2}$, $\mu = \frac{5}{2}$ states interacting only weakly with the conduction electrons through electrostatic and exchange interactions. The ordering of the $f$ orbital moments along the [001] easy-magnetization axis breaks the cubic symmetry introducing noncubic contributions to the potential seen by the conduction electrons. Because spin-orbit coupling in the conduction bands proves quite significant, the requisite model includes both the spin-orbit coupling and the polarization effects. The application of the model compares quite favorably with the measured de Haas—van Alphen frequencies except that the calculated polarization splittings, while quite small, are still overly large. It is found that the electron masses have little or no enhancement beyond the electron-phonon enhancement.

## I. INTRODUCTION

CeSb exhibits a very complicated magnetic phase diagram indicative of a delicate balance in its electronic structure. At low temperatures, the application of a strong magnetic field ($> 5$ T) will order the material as a simple ferromagnet with the moments pinned to a [100] easy axis of magnetization. It is thus possible to perform measurements on CeSb as a ferromagnetically ordered material. de Haas—van Alphen (dHvA) measurements on ferromagnetically ordered CeSb were first made by Kitazawa *et al.*[1] They were then interpreted using a *p-f* mixing model[2] in which the $f$ orbitals are assumed to be the origin of the magnetic moment but are sufficiently delocalized to hybridize with and thereby modify the conduction bands. Because a material with a single localized $f$ electron (rather than a multiplet shell) interacting with the conduction electrons is a very important system, Aoki *et al.*[3] have undertaken to make a very complete dHvA examination of CeSb in several of its magnetic phases. Their data for the ferromagnetic phase are reproduced in Fig. 1. The most interesting feature of the data is the lack of cubic symmetry. The frequency branch labelled $\alpha$ is particularly unusual as it appears to be the bottom half of the pattern of frequencies to be expected from a set of ellipses along the $\langle 100 \rangle$ directions. Equally interesting is the fact that the frequency branches labelled $\gamma$ would appear to be the top half of such a pattern but split off. The frequency branch labelled $2\alpha$ is almost certainty a second harmonic of the $\alpha$ branch[3] and is included only to make contact with the earlier results where this was not as clear. This harmonic can be especially misleading as it could easily appear to be the bottom portion of the $\gamma$ branches. Careful analysis,[3] however, reveals this not to be the case. The frequencies labelled $\beta$ are $\Gamma$-centered surfaces. The cutoff of the $\beta_1$ branch is probably due to the inability to detect the weak signal in the presence of two close-by and stronger signals. However, this branch does extrapolate nicely to the data point at the [110] direction. This experimental data base appears to be otherwise quite complete
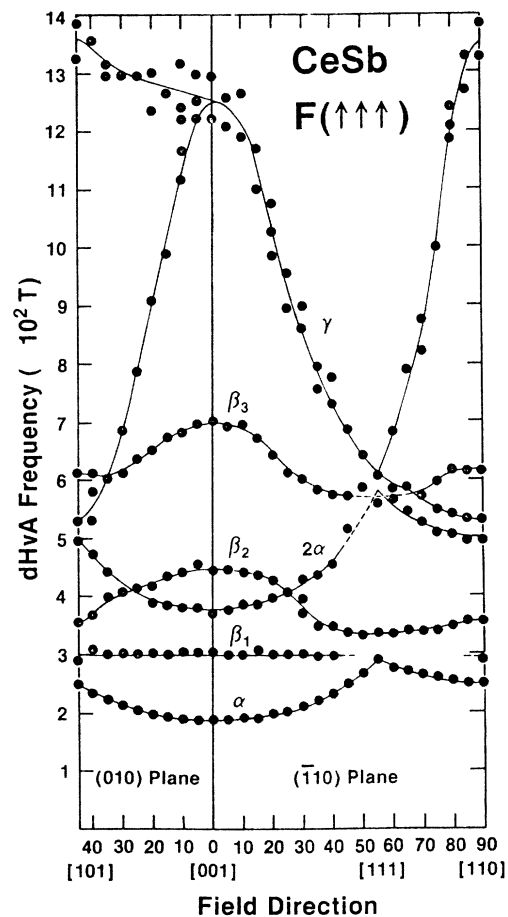


FIG. 1. Observed de Haas—van Alphen frequencies from Ref. 3. The $\alpha$ and $\gamma$ branches arise from ellipsoids along the [100] axes. The incomplete frequency patterns for these ellipsoids arise because the magnetic moments flip to follow the applied magnetic direction. The frequency labelled $2\alpha$ is the second harmonic of the $\alpha$ branch and is only included because this was not clear in the earlier data. The $\beta$ branches all arise from $\Gamma$-centered surfaces. It is assumed that the $\beta_1$ branch is incomplete only because of difficulties in observation.

and poses an excellent test to models of the electronic structure. It is further augmented by the less complete but very important effective mass data which are included in Table I.

In the course of the analysis of the newer data, it was seen that a number of difficulties arise when trying to interpret the data on the basis of the $p$-$f$ mixing model. These will be discussed below in light of the results to be presented. It would instead appear that CeSb—at least in its ferromagnetically ordered state—corresponds more closely to the standard model of rare-earth electronic structure in which there is only a very weak coupling between the localized $4f$ states and the sea of conduction

electrons. In the past, researchers have been principally interested in the behavior of the $f$ states under the influence of and coupled through the conduction electrons. Cooper and co-workers[4] have been studying CeSb from this point of view. In the present problem, however, the situation is reversed. The state of the $4f$ orbital is now fixed and its consequences on the conduction electrons are investigated. In this weak-coupling model, the primary coupling to the conduction electrons of the ordered localized $f$ states is assumed to be a crystal field arising from electrostatic and exchange interactions while the $p$-$f$ hybridization is assumed to be much weaker and is, at least initially, ignored.

TABLE I. Theoretical and experimental cross-sectional areas and masses for CeSb. Data are given along the three principal symmetry directions for the three calculations: the spin-polarized calculation with no conduction electron spin-orbit coupling (SP-vBH), the spin-orbit coupled conduction-band calculation (full SO-vBH), and the two spin-orbit coupled conduction-band calculations with different exchange-correlation functionals but the spherical polarization effects omitted (SO-vBH and SO-KSG). The experimental results of Aoki et al. (Ref. 3) are reproduced for comparison. The data are given together for the polarization split pairs. Areas are given in megagauss and masses in electron masses.

| | [011] | | [001] | | [111] | |
|---|---|---|---|---|---|---|
| | $A$ | $m^*$ | $A$ | $m^*$ | $A$ | $m^*$ |
| | | | SP-vBH | | | |
| (1,1') | (4.31,4.63) | (−0.12,−0.12) | (4.21,4.58) | (−0.11,−0.12) | (4.31,4.62) | (−0.12,−0.13) |
| (2,2') | (7.55,8.02) | (−0.26,−0.27) | (8.89,9.23) | (−0.36,−0.37) | (7.04,7.50) | (−0.21,−0.22) |
| (3,3') | (10.15,11.68) | (−0.34,−0.37) | (11.10,13.13) | (−0.39,−0.44) | (8.94,9.94) | (−0.26,−0.28) |
| (4,4') | (3.41,2.48) | (0.29,0.23) | (2.10,1.57) | (0.18,0.15) | (4.45,3.24) | (0.35,0.29) |
| | (5.42,4.70) | (0.47,0.45) | (24.22,23.23) | (0.75,0.76) | (6.81,5.88) | (0.57,0.54) |
| | (26.96,24.84) | (1.10,1.07) | | | | |
| | | | Full SO-vBH | | | |
| (1,1') | (3.01,3.39) | (−0.18,−0.16) | (3.23,3.66) | (−0.18,−0.17) | (2.92,3.30) | (−0.18,−0.16) |
| (2,2') | (5.55,5.84) | (−0.30,−0.30) | (5.98,6.02) | (−0.31,−0.30) | (5.14,5.51) | (−0.27,−0.28) |
| (3,3') | (8.02,9.27) | (−0.40,−0.45) | (9.88,11.55) | (−0.53,−0.61) | (7.48,9.07) | (−0.32,−0.34) |
| (4,4') | (3.97,2.78) | (0.25,0.19) | (2.92,2.08) | (0.17,0.13) | (4.65,3.23) | (0.29,0.22) |
| | (5.15,4.14) | (0.33,0.30) | (9.84,8.63) | (0.56,0.56) | (5.99,4.85) | (0.37,0.35) |
| | (10.11,8.25) | (0.67,0.60) | | | | |
| | | | SO-vBH asymmetric components only | | | |
| (1,1') | (3.02,3.40) | (−0.18,−0.16) | (3.25,3.67) | (−0.18,−0.16) | (2.94,3.30) | (−0.18,−0.16) |
| (2,2') | (5.34,6.00) | (−0.31,−0.29) | (5.53,6.42) | (−0.31,−0.31) | (5.01,5.58) | (−0.29,−0.26) |
| (3,3') | (8.12,9.12) | (−0.43,−0.42) | (9.76,11.69) | (−0.55,−0.57) | (7.92,8.50) | (−0.34,−0.31) |
| (4,4') | (3.50,3.20) | (0.22,0.21) | (2.58,2.37) | (0.16,0.15) | (4.10,3.74) | (0.26,0.25) |
| | (4.94,4.37) | (0.32,0.31) | (9.98,8.64) | (0.57,0.54) | (5.74,5.11) | (0.36,0.36) |
| | (9.75,8.69) | (0.65,0.62) | | | | |
| | | | SO-KSG asymmetric components only | | | |
| (1,1') | (3.13,3.52) | (−0.18,−0.16) | (3.36,3.81) | (−0.19,−0.17) | (3.04,3.42) | (−0.18,−0.16) |
| (2,2') | (5.40,6.08) | (−0.31,−0.29) | (5.58,6.47) | (−0.31,−0.30) | (5.04,5.61) | (−0.29,−0.27) |
| (3,3') | (8.40,9.32) | (−0.43,−0.42) | (10.09,11.88) | (−0.54,−0.55) | (8.38,8.95) | (−0.35,−0.32) |
| (4,4') | (3.65,3.36) | (0.23,0.22) | (2.68,2.47) | (0.16,0.16) | (4.28,3.93) | (0.27,0.26) |
| | (5.07,4.49) | (0.32,0.32) | (10.08,8.73) | (0.57,0.54) | (5.88,5.24) | (0.37,0.37) |
| | (9.86,8.78) | (0.65,0.62) | | | | |
| | | | de Haas—van Alphen (Ref. 3) | | | |
| 1 | 3.0 | | 3.0 | −0.50 | 3.0 | |
| 2 | 3.6 | −0.56 | 4.4 | −0.97 | 3.3 | |
| 3 | 6.2 | −0.65 | 6.9 | −0.89 | 5.6 | |
| 4 | 2.5 | 0.31 | 1.9 | 0.23 | 2.9 | |
| | 5.3 | 0.49 | (12.2,12.9) | (0.94,0.82) | 6.0 | 0.53 |
| | (13.2,13.9) | (1.00,0.90) | | | | |

The primary objective here will be to establish the credibility of this model for CeSb. To do so, an approximate density-functional theory will be applied using almost standard band-theory techniques to determine the Fermi-surface topology. Several caveats are required which are presented in Sec. II where the model is discussed in more detail. The details of implementation, which are also a significant consideration, are separately presented in Sec. III. The results are presented in Sec. IV where they are compared with the de Haas—van Alphen data of Aoki et al.[3] Results are also presented for a calculation on LaSb. This has been included both to assay the precision of the functionals used and to provide a basis for comparison to the p-f mixing model which utilized a knowledge of the LaSb bands to discuss the bands of CeSb. In Sec. V, we discuss the results.

## II. THE WEAK-COUPLING MODEL

To formulate this weak-coupling model, one starts from the basic observation that the Ce $4f$ orbitals order ferromagnetically in sheets perpendicular to a [100] direction. Relative to that [100] direction, the $4f$ orbital is in a $j = \frac{5}{2}$, $\mu = \frac{5}{2}$ state and there is a strong anisotropy pinning the moments and sheets along the axis. At low magnetic fields, this is a ferromagnetic system with a nine-plane repetition length; at intermediate fields, the repetition distance is reduced to three planes; and at high fields above roughly 5 T, the material orders ferromagnetically. It is this high-field configuration which will be investigated here. The mechanism of this ordering is a separate, although not unrelated, problem that will not be dealt with here. The existence of these ordered moments breaks the cubic symmetry. The $\mu = \frac{5}{2}$ orbital has the axial symmetry of an oblate spheroid so the system contains an ordered array of pancakelike densities arising from the $4f$ orbitals. This produces the noncubic properties observed with the dHvA measurements that are the primary focus of both the current weak-coupling model and the previous p-f mixing model.

In both models, it is the lower symmetry of the ordered $4f$ orbitals that drives the reduced symmetry of the system. The difference between the two models is the manner in which the coupling to the conduction electrons occurs. The p-f mixing model assumes wave-function hybridization while the current weak-coupling model achieves the coupling through a potential interaction. This weak-coupling model is actually the application of a standard rare-earth-like picture where the $4f$ orbitals are viewed as site-local atomiclike orbitals interacting with the conduction electrons only through electrostatic and exchange interactions. The exchange interactions are included using the local-density approximation (LDA) so the symmetry properties are not further modified. Hybridization between the $4f$ orbitals and the conduction electrons—the major interaction assumed in the p-f mixing model—is neglected. This property is not adequately described by density-functional theory within the local-density approximation so a straightforward band calculation including the $4f$ states as band states will find significant hybridization. This, however, is a limitation of the local-density approximation which is being actively investigated.[5] For now, the nonhybridization of the $f$ states will be merely taken as an assumption of the weak-coupling model. It should also be noted, of course, that the noncubic $4f$ charge density also results in a tetragonal distortion of the lattice as well. But while the distortion of the lattice is significant, elementary estimations of its effect on the Fermi surface indicate it is unable to cause the modifications actually observed and so will be considered of second order.

Operationally, the application of the weak-coupling model requires that one perform a modified self-consistent band-structure calculation in which the single $4f$ orbital is treated like an incompletely occupied core state. This means that it is solved as a single-site orbital (with some minor adjustments at large $r$) and included with a fixed occupation. The density arising from this set of orbitals—one per site—is then merely added into the density which is used in a standard density-functional expression. Several approximations have been made in the current calculations to ease the computational effort. The actual self-consistent calculations were carried out ignoring the nonspherical terms which are the basis of the symmetry breaking. This allows the exploitation of cubic symmetry during the time-consuming process of achieving self-consistency. Once self-consistency has been achieved for the simplified problem, the nonspherical terms are introduced as a perturbation. One may expect that this will be a reasonably adequate treatment of these terms. One also may predict that any error in the procedure should result in the prediction of too large an effect since perturbative corrections normally overshoot.

Several calculations were performed with the $4f$ orbitals treated as Bloch orbitals in contrast to the assumed model. This was done to explore the effect of violating the assumption of the local orbital behavior of the $4f$ states. It will be seen below that the Fermi surface cannot be properly represented in this way. However, except for the fact that the Fermi surface is not reproduced, the results of the calculation appear quite reasonable and show significant $4f$-conduction electron hybridization. This is most likely evidence of a limitation in the LDA. The LDA to the exchange-correlation potential is known to work well for most noninsulating solids. Unfortunately, for localized electrons, the LDA does not work nearly as well. Good approximations to the exact density-functional potential are known for atoms[5,6] but these potentials are implicit functionals of the charge density as opposed to explicit functionals (such as LDA) so they are difficult to construct for solids. Generally, though, LDA charge densities compare fairly well with those of the more involved functionals except in those cases where the LDA predicts the wrong ground state. This occurs, for example, in several transition-metal atoms where the LDA energy functional actually minimizes at noninteger occupation number (i.e., for Fe at $d^{6.4}s^{1.6}$). The improved functionals correctly predict integral orbital occupation numbers.[5] This feature is closely related to the overestimation of hybridization by the LDA and one suspects strongly that, were one able to include an improved exchange-correlation functional, the calculated hybridiza-

tion would be drastically reduced. At present, however, a reasonable approach is to artificially put the dehybridization into the model and proceed to explore its consequences under the observation that the LDA will give reasonable results given the "correct" ground state. In doing this, one is actually seeking the ground state of a constrained system much as is done for atoms. It is not clear that one has a best choice for the form of the exchange-correlation functional when this is done. Thus, to test the sensitivity to choice of functional, calculations were performed with both exchange-only [Kohn-Sham-Gaspar (KSG)] and von Barth—Hedin (vBH) (Ref. 7) functionals. (This is especially appropriate as the Fermi energy is near the bottom of the Ce $d$ bands and limitations of the LDA have been observed in that regime for the transition metals.)

There is yet one further dilemma to be faced for this material: Both polarization and spin-orbit effects are significant. A formal solution has yet to be worked out for this situation in a solid. It would seem clear that the $4f$ orbital should be treated in a $j = \frac{5}{2}$ state with ordered moment. That is the assumption of the model. In all local orbital calculations, the $4f$ orbital was treated as a $j = \frac{5}{2}$ orbital. To represent a $j = \frac{5}{2}, \mu = -\frac{5}{2}$ state as a spin density, $\frac{6}{7}$ of the electron is placed in an up-spin state and $\frac{1}{7}$ of the electron in a down-spin state. These ratios were obtained from the appropriate Clebsch-Gordan coefficients. [Note that the majority (up) spin is opposite in direction to the resulting moment since the orbital moment is opposite to the spin moment.]

But there is still the question of the best way to deal with the conduction electrons. Should one include spin polarization first and then add some spin-orbit coupling, or should one focus first on the spin-orbit coupling? To study this question, both spin-polarized calculations and spin-orbit calculations were performed. It was found that the polarization effects were small (although not so small as implied by the dHvA data) and it was much more important to include the spin-orbit effects because they split the band degeneracy at the $X$ point and cut off the electron ellipsoids there. The small size of the spin splitting is a difficult consideration for the application of the $p$-$f$ mixing model because it assumes that the spin splitting is very large.

## III. CALCULATIONAL PROCEDURES

All calculations utilized the linearized augmented plane-wave (LAPW) method.[8] The semirelativistic approximation[9] which includes all kinematic relativistic effects except spin-orbit coupling was used throughout all the calculations. When spin-orbit coupling was included, it was incorporated in a second variational step based on reinsertion of spin-orbit coupling into the semirelativistic analysis.[10] Except when the nonspherical effects of the $4f$ orbitals were introduced, all calculations were performed using the warped-muffin-tin (WMT) shape approximation. In this approximation, the density and potential are spherically averaged within muffin-tin spheres about each atomic site. In the interstitial region between these spheres, the proper variation was described using a sym-

metrized plane-wave expansion. CeSb crystallizes in a rock-salt structure with a lattice constant of 12.1 atomic units. As equal-sized spheres were used, the muffin-tin sphere radius within which this spherical averaging occurred with 3.025 a.u.

Reasonable care was taken to ensure adequate precision of the self-consistent calculations. The basis functions were selected for each $k$ point by including all augmented plane waves (APW's) where the magnitude of the wave vector times the muffin-tin radius was less than or equal to 8—i.e., $kR_{max} = 8$. This results in 137 basis functions at the center of the Brillouin zone. The Brillouin zone was sampled on a $\pi/4a$ cubic mesh. This is the standard 89-point mesh (only 85 of which are actually independent). When the tetragonal symmetry terms of the Hamiltonian were included, the number of inequivalent points was increased by almost a factor of three to 205 points. (It was not precisely three because some points exist on the planes joining the volumes which become inequivalent in the tetragonal symmetry.) The densities were determined from the wave functions calculated on this mesh. The eigenvalues, however, were linearly interpolated and used with a tetrahedron-based integration scheme[11] to determine a more precise density of states. This interpolation was also used to modify the weighting of the density arising from a given band at that $k$ point by the Fermi-factor occupation of the volume within a cube centered on the point. Core states were not held frozen but solved for at each iteration in a single-site approximation. The Sb $5s$ and Ce $5p$ semicore states, however, extend sufficiently beyond the muffin-tin radius that they were included using LAPW solutions just like the valence- and conduction-band states. Self-consistency iterations were continued until the maximum change of any eigenvalue from one cycle to the next was less than 0.1 mRy.

The procedures outlined thus far are rather standard techniques and need very little elaboration. The inclusion of the anisotropic effects of the $4f$ orbitals, however, is more unusual and requires description in somewhat greater detail. The $4f$ orbital was treated as a local orbital in the $j = \frac{5}{2}, \mu = -\frac{5}{2}$ state. To avoid including them twice, the itinerant $4f$ states were excluded by placing the $l = 3$ LAPW energy parameter in the $5f$ energy region thereby removing all variational freedom to resolve the $4f$'s from the basis set. The choice of the negative $\mu$ state was to orient the majority spin, which is oriented opposite to the total moment, in the positive sense. The upper two components of the $4f$ orbital are then

$$
\begin{bmatrix}
c\,(3, \frac{1}{2}, \frac{5}{2}; \overline{3}, \frac{1}{2}, \frac{\overline{5}}{2})g\,(r)Y_3^{-3}(\hat{r}) \\
c\,(3, \frac{1}{2}, \frac{5}{2}; \overline{2}, \frac{\overline{1}}{2}, \frac{\overline{5}}{2})g\,(r)Y_3^{-2}(\hat{r})
\end{bmatrix} .
$$

The radial solution $g\,(r)$ was obtained by extrapolating the Ce muffin-tin potential to larger radii and then utilizing the same technique as is used for the core orbitals. This yielded an orbital 0.3 eV below the Fermi energy. The actual choice of extrapolation had little effect as only 1% of the orbital extends beyond the muffin-tin radius. The spin densities produced from this wave function are

$$\rho_{f\uparrow}(r) = \frac{1}{4\pi} \frac{6}{7} g^2(r)[1 - \tfrac{5}{2}P_2(\hat{r}) + \tfrac{9}{11}P_4(\hat{r}) - \tfrac{5}{33}P_6(\hat{r})] \ ,$$

$$\rho_{f\downarrow}(r) = \frac{1}{4\pi} \frac{1}{7} g^2(r)[1 - \tfrac{21}{11}P_4(\hat{r}) + \tfrac{10}{11}P_6(\hat{r})] \ .$$

The $\tfrac{6}{7}$ and $\tfrac{1}{7}$ factors are the squares of the Clebsch-Gordan coefficients and the Legendre polynomial expansions are the squares of the spherical harmonics. In performing the local orbital WMT calculations, these series are merely truncated at the first (spherically symmetric) term. The effects of current interest are the consequence of including these additional nonspherical—and also noncubic—terms. The resultant change in the electrostatic potential can be obtained using standard multipole-field techniques based on the expansion of $1/|\mathbf{r}-\mathbf{r}'|$ as

$$\frac{1}{|\mathbf{r}-\mathbf{r}'|} = 4\pi \sum_{l=0}^{\infty} \frac{1}{2l+1} \frac{r_<^l}{r_>^{l+1}} \sum_{m=-l}^{l} [Y_l^m(\hat{r})]^* Y_l^m(\hat{r}') \ .$$

The form of this expansion together with the orthonormality of the spherical harmonics dictates that the site symmetry of the resultant potential change $\Delta V$ will be the same as that of $\rho_f$. The same is true for the exchange corrections which were obtained using a Taylor-series expansion about the spherical density. We chose to truncate the series at the linear term so $\Delta V_x$ is directly proportional to $\Delta\rho_f$ but the symmetry would not be further modified by the inclusion of higher-order terms of the expansion. Nonspherical corrections to the correlation functional were not included as they were much smaller. For the Ce atomic sites, only the site-diagonal potential effects were retained and these were truncated at $L=4$. The $L=6$ potential term is quite small and can have little effect since most of the $f$ character is to be found in the local $4f$ orbital. (The $l=3$ character remaining in the conduction bands was included by giving the basis functions orthogonal $5f$ and $5f$-derivative character.) The site-local interaction is based on the rapid decay of the multipole fields. The weakest case is for the quadrupole term $(L=2)$ which decays as $1/r^3$. We did include the effect of this field on the nearest-neighbor Sb atoms as the longest-range interaction. To thus include the effect of the quadrupole terms from the six nearest-neighbor Ce sites on the Sb site, it was necessary to reexpand the $1/r^3$ about the Sb site. Only the $L=2$ term at the Sb site needed to be considered as the higher-order terms were quite small. The effects of these terms were small being of the same order as the $L=4$ terms on the Ce site. It was the $L=2$ term on the Ce site which produced the major effect.

These effects were incorporated by performing a second variation[12] utilizing the eigenvectors resulting from the WMT calculation as a basis set. The set chosen was the first eight bands above the Ce $5p$ and Sb $5s$ bands—the predominantly Sb $5p$ and Ce $5d$ bands. The spin-orbit coupling was also included by the same technique so it would have been possible to include both effects simultaneously. We instead chose to include them serially but, since there was no truncation, this was just a matter of convenience. To perform such a second variation, it is necessary to set up and solve a secular equation involving matrix elements which are bilinear products of the eigen-

vectors of the WMT equations with the LAPW matrix elements of $\Delta V$. The LAPW matrix elements of $\Delta V$ are evaluated using the spherical harmonic representation of the LAPW's truncated at $l=3$. Because there are no nonzero $m$ terms in $\Delta V$, the resultant coupling is diagonal in $m$. The quadrupole $(L=2)$ term gives $p$-$p$, $d$-$s$, $d$-$d$, $f$-$f$, and $p$-$f$ coupling. The $L=4$ term gives $d$-$d$, $f$-$f$, and $p$-$f$ coupling. Note that the $L=6$ term omitted would only have given $f$-$f$ coupling. To facilitate the study of the Fermi surface, a plane-wave-series spline fit was used.[13] This was done in the tetragonal symmetry case so the $\pi/4a$ cubic mesh corresponds to 205 inequivalent points. 366 symmetrized (star) functions were then used to represent the results by requiring the fit to go through all data points and also be as smooth as possible. This plane-wave-series representation was then used to trace out the orbits on the Fermi surface.

## IV. RESULTS

When the $f$ electrons were treated as Bloch states, flat $f$ bands resulted at and just above the Fermi energy. These bands repelled the $p$-$d$ bands below the Fermi energy and the resulting Fermi surface had no relation whatsoever with the experimental areas shown in Fig. 1. Further, such bands exhibit very large effective masses whereas the experimentally determined masses were all quite small. It is, of course, to be recognized that that calculation omitted many of the effects being advanced as the essential physics; it is a spin-polarized calculation, so the $4f$ orbital is included as a definite spin state rather than as a $j=\tfrac{5}{2}$ spin-orbit coupled state and the tetragonal symmetry terms have not been allowed. However, the fact that the observed effective masses are so low makes it improbable that even after including these corrections one would find acceptable results with delocalized $4f$ states since they would be pinned at the Fermi energy with their attendant large mass.

As the $p$-$f$ mixing model assumed a large exchange splitting, the first calculations performed for the local $4f$ orbital case neglect the spin-orbit coupling and start from a spin-polarized calculation except the $4f$ orbital is in the $j=\tfrac{5}{2}$, $\mu=-\tfrac{5}{2}$ state as described above. When the nonspherical components of the $4f$ orbital density are neglected, the symmetry of the system is still cubic and a WMT self-consistent-field (SCF) calculation can be performed as an fcc-like (rock-salt) system. This is to be referred to as the base calculation. The resultant spin-up bands are shown in Fig. 2. The spin-down bands are quite similar. The nonspherical terms are then included via a second variation after the last cycle. The resultant model is identified as the spin-polarized (SP) calculation. In Fig. 3, the spin-up Fermi-surface areas are shown for this model. Table I gives the actual areas and masses for the principal symmetry directions together with the experimental values[3] for comparison. The spin-down areas have not been shown in the figure because, contrary to the assumptions of the calculation, they are quite similar. One sees orbits from three-hole surfaces centered at $\Gamma$ $(\beta_1,\beta_2,\beta_3)$ and from cigar-shaped electron ellipsoids centered at $X$ (the $\alpha$ orbit around the belly of the ellipsoid and the $\gamma$ or-
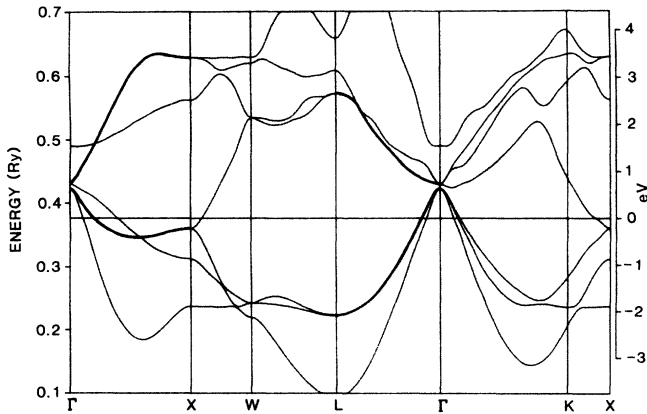
FIG. 2. Band structure for the spin-up bands of the spin-polarized base calculation with the $4f$ orbitals treated as local states. The noncubic terms arising from the $4f$ orbital are not present at this stage. Although they break the symmetry, they will make only minor modifications to the bands shown. The spin-down bands (not shown) differ only slightly from the spin-up bands.

bit that goes around the major axis). Each of these orbits can be seen to correspond to frequencies in the experimental data (Fig. 1). They generally exhibit the correct anisotropy except that the calculated areas are too large for the hole orbits and the electron orbits are too needlelike. The
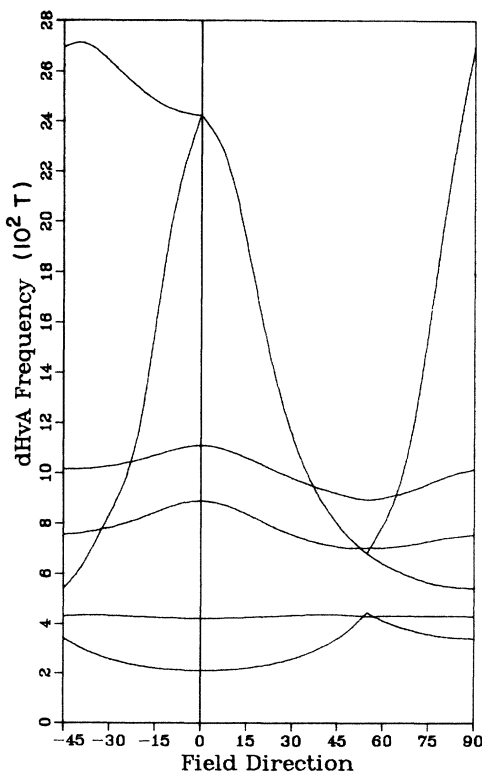


FIG. 3. Extremal cross sections arising form the SP spin-up bands with the noncubic terms included. The spin-down areas will be very similar—but distinct.

mysterious $\alpha$ orbit now occurs as a consequence of the noncubic terms, because of the moment alignment along an [001] axis, the ellipsoid around the $\Gamma$ axis in that direction has a smaller belly cross section than the two in the perpendicular direction. Thus that orbit "disconnects" and forms the $\alpha$ orbit. The reason that the entire pattern of frequencies associated with an ellipse is not seen for each of these now different ellipses is that the moment direction flips to a new [100] direction when the field direction is moved too far off axis so that only a limited part of each ellipsoid can be observed. There is a second set of frequencies arising from the spin-down bands which are very similar to, but distinct from, the spin-up bands. This is not seen experimentally but there is some evidence of very small splittings in the data. A splitting of only 0.7 MG is observed for the large $\gamma$ electron frequencies, less than predicted by the model. Thus if one assumes that other predicted splittings, already small, have actually been overestimated by the calculation, then the true splittings would indeed be too small to be distinguished in the experiment except in the largest cases.

It is very reasonable to ask whether the spin-orbit coupling, which has been omitted for the conduction bands in the SP model, might not reduce the spin splitting. To test this, a second model was constructed which omitted the spin polarization from the base calculation and included spin-orbit effects instead. The base calculation for this spin-orbit model (SO) was created by first performing a paramagnetic WMT SCF calculation (without spin orbit) with the $4f$ density split evenly between the two spin states. Only at the last cycle was the spin-orbit coupling included to form the basis for the new calculation. The resulting band structure is shown in Fig. 4. This should be an adequate treatment of spin-orbit effects since the $4f$ orbital is not a part of the conduction bands. To complete this model, the nonspherical components and polarization
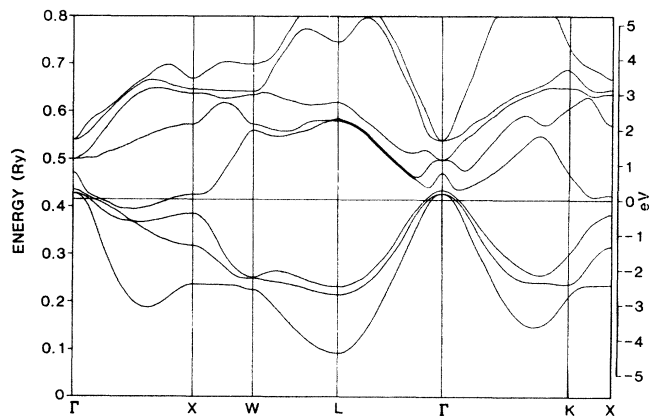


FIG. 4. Band structure for the spin-orbit coupled paramagnetic bands. The anisotropic and exchange-splitting terms of the $4f$ state are not yet included in this base calculation so the bands are all doubly degenerate. A very important feature to note in comparison to the spin-polarized bands of Fig. 2 is that the spin-orbit coupling has moved band 4 above the Fermi energy at $X$ thereby pinching off the ellipsoids there.

of the $4f$ orbital were included in a final variational calcu-
lation using the spin-orbit coupled solutions of the WMT
problem as a basis set. Because these interactions break
the spin-flip symmetry (by the polarization), all states
couple and the degeneracy is gone. The second-variation
secular equation is twice the size and all bands are found
at once. This is in contrast to the SP case where the spins
are decoupled. It should be noted that this is still a polar-
ized calculation (being driven by the $4f$ polarization).
However, it will be a linear response to that driving force
that allows no self-consistent relaxation or screening. As
such, it will also overestimate the polarization effects.

The resultant areas for this SO calculation are shown in
Fig. 5 with the symmetry direction results tabulated in
Table I. The agreement with experiment is greatly im-
proved over that of the SP calculation. The hole orbits
are smaller although still larger than the experimental fre-
quencies. But the most dramatic change is in the electron
ellipsoids. The spin-orbit coupling has lifted the degen-
eracy of bands 3 and 4, forcing band 4 above the Fermi
energy at $X$. This pinches off the ellipsoids at $X$ such that
they have a new center along $\Delta$. (This can be seen by
comparing Fig. 2 and Fig. 4 which exhibit the base calcu-
lations for the SP and SO models.) Simultaneously, the
ellipses have become much bigger at the waist so the an-
isotropy is drastically reduced. The calculated results
have actually gone too far in this direction and are now
somewhat less anisotropic than the experimental frequen-
cies. As can be seen from Table I, the spin splittings of
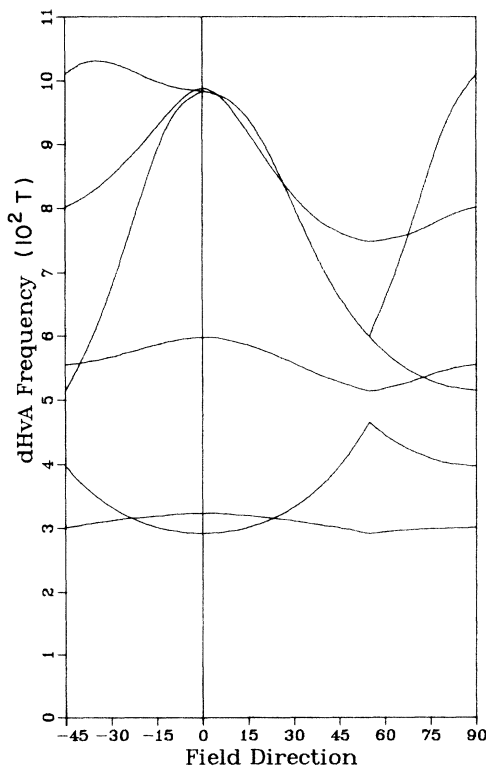
the SO calculation are quite comparable to those of the SP
calculation—in some cases they are even larger. To get an
estimate of the polarization effects from the data given in
Table I, we can use the effective mass relation

$$m^* = \frac{1}{\pi} \frac{dA}{dE} \ ,$$

which is in atomic units. Converting $m^*$ to effective
mass ratio ($m_e = \frac{1}{2}$), areas to megagauss [(374.1 MG)
a.u.$^2$], and to millirydberg energies, this becomes

$$\Delta E = (1.7017/m^*)\Delta A \ .$$

When this simple relation is applied to the data in Table I,
one finds that the splittings are 4–5 mRy with no clear
difference between the SP and SO calculations. The signi-
ficance of this is that the spin-orbit splitting of the con-
duction bands has not greatly reduced the polarization ef-
fects and the self-consistent polarization screening present
in the SP calculations and not in the SO calculations has
had at least as large an effect. To further probe this re-
sult, a modified spin-orbit calculation was performed in
which the spherically symmetric component of the polari-
zation was omitted. The results, also tabulated in Table I,
showed that the spherical component of the polarization
had very little effect at all.

To test the effect of the assumed exchange-correlation
functional on the results, the SO calculation was repeated
using exchange only (KSG). This should give the largest
change possible without going beyond the LDA since the
various exchange-correlation parametrizations are quite
close compared to the size of the correlation effects. The
results are tabulated in Table I. They do not differ greatly
from the vBH results although they are somewhat worse.
The $p$-$f$ mixing model extrapolated the band results for
LaSb to represent also the conduction bands of CeSb be-
fore the $4f$ hybridization. This is a venerable rare-earth
technique and worthy of examination. At the same time,
one can also get some estimate of the reliability of the cal-
culations for the nonpolarized conduction bands. To do
this, a paramagnetic band calculation with spin-orbit cou-



FIG. 5. Extremal cross-sectional areas resulting from the SO
calculation with the noncubic and exchange polarization effects
included (only one set of exchange-split bands are shown).
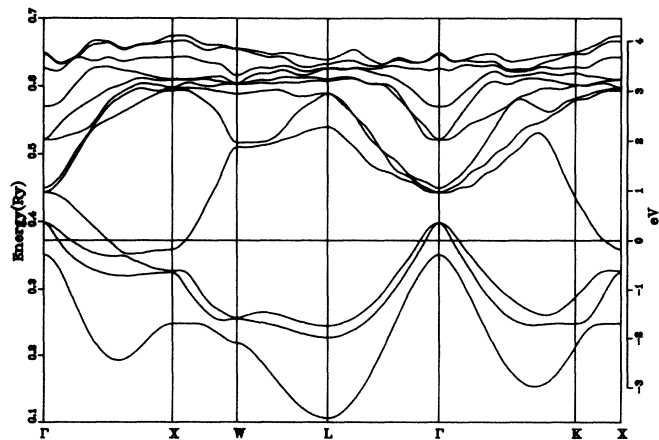


FIG. 6. Band structure for the spin-orbit coupled bands of
LaSb. Note the differences from the local $f$ CeSb bands of Fig.
4.

TABLE II. (100) orbital areas and masses for LaSb. Areas are in megagauss and masses (given in parentheses) are in electron masses. Experimental data are from Ref. (1).

|            | Band 2       | Band 3         | Band 4        | Band 4-waist |
|------------|--------------|----------------|---------------|--------------|
| dHvA data  | 4.41         | 11.03          | 8.27          | 2.17         |
| SO-KSG     | 5.43 (−0.25) | 14.54 (−0.65)  | 11.86 (0.72)  | 1.51 (0.26)  |
| No SO-KSG  | 7.20         |                | 12.83         |              |

pling was performed for LaSb in precisely the same manner as for CeSb. The exchange-only (KSG) functional was used resulting in the bands shown in Fig. 6. Only two-hole surfaces are seen at $\Gamma$ since spin-orbit splitting causes band 1 to fall below $E_F$ (note this does not occur for the local $f$ CeSb calculation). There is an electron ellipsoid at each $X$ point (the local $f$ SO CeSb calculation had the ellipsoids centered halfway between $\Gamma$ and $X$). The reason for this difference between LaSb and CeSb is that the $d$ bands in CeSb are lower than in LaSb. The resulting Fermi-surface areas are compared to the experimental areas of Ref. 1 in Table II. Using the effective mass formula again, one finds that the bands generating the ellipses at $X$ are too low by about 9–10 mRy relative to the hole bands at $\Gamma$ and that the ellipsoidal surface is much too anisotropic, being more needlelike than the observed frequencies. The point here is that the quantitative differences found for CeSb are also found for LaSb indicating that these are due to the approximation of the band calculation as opposed to the validity of the local $f$ model. The major approximations are (i) neglect of nonspherical terms inside the muffin-tin spheres (WMT), (ii) overestimation of spin-orbit splitting effects because they were not included in the self-consistency process, and (iii) use of the LDA for the exchange-correlation (XC) potential. Approximation (iii) is certainly a critical one. It is known from calculations on early transition metals such as niobium[14] and vanadium[15] that the electron ellipsoids are too large due to the use of the LDA. In these elements, the $d$ states are placed too low relative to the $s$-$p$ states. For a discussion of the effect of different XC potentials as well as shape approximations to the total potential on an isoelectronic compound LaN, the reader is referred to Ref. 16. With the above observations on LaSb in mind, relative shifts between the $d$ and $p$ states were tried on CeSb. A shift of the $d$ states upwards by 10 mRy was found to have little effect, merely resulting in a small reduction in the eccentricity of the ellipsoids.

## V. DISCUSSION

The application of the $p$-$f$ mixing model to CeSb is based on the use of LaSb bands as an approximation to the unhybridized CeSb conduction bands. This is a standard approximation used in dealing with rare-earth materials but, although correct in gross structure, it unfortunately does not adequately represent a number of features relevant to the problem at hand. The unhybridized CeSb calculation has three-hole surfaces at $\Gamma$ because band 1 is above the Fermi energy there. A particularly difficult problem for the $p$-$f$ model is that these bands are predominantly Ce-$d$ derived rather than Sb-$p$

derived as assumed by the model. As these are the bands assumed to be modified by $p$-$f$ mixing, it is a very severe problem that there be no $p$ character in the bands. Next, the $p$-$f$ model places the $f$ orbital about 1 eV below the Fermi energy. This is also a necessary part of the $p$-$f$ mixing model since the $p$-$f$ interaction is being used to force a band above the Fermi energy by repulsion. Recent optical data, though, indicate that the $f$ levels are less than 0.5 eV below the Fermi energy.[17] The calculations presented here found it at about 0.3 eV below the Fermi energy. Further, the $p$-$f$ mixing model assumes a very large polarization splitting to eliminate the spin-down bands which it assumes are not seen. But a small splitting has now been detected in the dHvA data[3] and the calculations presented here found splittings of 4–5 mRy, more in line with those found in other materials. Finally, the $p$-$f$ mixing model generates the $\alpha$ orbit as a neck on the largest $\Gamma$ surface along the field or moment direction because of the anisotropy of the $4f$ orbital. But the newer dHvA data show this frequency to exist at all orientations. They also show no evidence for an orbit around a large-hole surface. So although the $p$-$f$ mixing model is an appealing hypothesis, all this taken together would rule against the applicability of the $p$-$f$ hybridization model as it is applied to CeSb.

The weak-coupling model assumes instead that $4f$-orbital localization is complete in CeSb. This makes CeSb a very interesting rare-earth-like system with the local $f$ shell consisting of *only one single 4f orbital*. The noncubic anisotropy is also driven by the ordered $4f$ orbitals but the interaction is now through direct and exchange Coulomb effects. Consequently, the placement of the energy of the $4f$ orbital is not critical. The splitup of the $\alpha$ and $\gamma$ orbits is due to the ellipsoid along the field (moments) being reduced in size and the two transverse ellipsoids being enlarged. The full pattern of frequencies is not seen for these ellipsoids because as the magnetic field is oriented too far from the [100] axis of the moment alignment the moment alignment will flop to the closer [100] axis. This field dependence is certainly simpler than that observed for Ni (Ref. 18) but it is clear that the applied field is modifying the system—after all, it would not even be ferromagnetic if the field were not applied. The current application of this weak-coupling model has been quite satisfactory. It was found that the primary effect of spin-orbit effects in the conduction bands was to split bands 3 and 4 at $X$ ($X_5$), moving band 4 above the Fermi energy at $X$ and thereby pinching off the ellipsoids at $X$. Exchange-polarization effects on the conduction bands were found to be quite small, consistent with such effects being just barely detectable in the dHvA data. The calculated splitting nonetheless appears to be too large. There are at least

three possible explanations for this. (i) The existence of the $4f$ quadrupole density should drive the conduction electrons out of the plane of the $4f$ orbital thereby reducing the exchange interaction. Because the current application of the model has not allowed relaxation of the conduction electrons to the nonspherical driving force from the $4f$ orbitals, this effect is not present in the current application. The observation that the principal exchange-splitting effects arise from the anisotropic components strongly suggests that this must be at least part of the correct explanation. (It is well known that perturbative corrections overshoot.) (ii) The anisotropy of the correlation part of the exchange-correlation functional has been neglected. Correlation is well known to drastically reduce the spin dependence of this functional so the proper inclusion of these terms cannot but reduce the splitting. (iii) The nature of the ordered $4f$ orbital has been assumed as a $(j = \frac{5}{2}, \mu = -\frac{5}{2})$ state. Crystal field, orthogonalization, and hybridization (if present) effects could also act to reduce the spin polarization of the orbital. Parenthetically, the reader should note that we are being required to discuss reducing already small exchange effects while retaining the direct Coulomb effects. This is just the opposite of what would be assumed for a Kondo model.

The effective mass data given in Table I are quite interesting in that the masses and the mass enhancements are relatively small. To belabor a point, were there to be significant $f$ admixture into the conduction bands, one would expect large masses. Further, as the transition to localized behavior is approached from the itinerant side, mass enhancements become quite large. The mass-enhancement factors seen in CeSb appear to be roughly 2–3 which is quite comparable to the factor of 2 for LaSb as derived from a comparison of the density of states to the electronic specific-heat coefficient. Although that comparison is troubled with large uncertainties, it strongly suggests that the enhancements seen for CeSb are mostly derived from the electron-phonon interaction. This is again consistent with CeSb, being very like the standard weak-coupling rare-earth model.

To close, we would like to offer the opinion that CeSb, acting much like a standard rare-earth system rather than like the more exotic mixed-valent-cerium materials, is nevertheless an exciting system. Here one has a rare-earth material where the $f$ shell consists of a single electron rather than a more complicated many-body system. The material can be made very pure and very perfect—evidence the ability to detect a dHvA signal which is sensitive to parts per million. Thus it offers the opportunity to have very-well-controlled experiments on a system which is a relatively simple example of a most significant class of materials. It will definitely be desirable to improve our treatment of this material and explore the level of agreement which can be achieved between experiment and theory for this material. Clearly, the first step in improving the application of the basic model without interactions will be to include the nonspherical response of the conduction electrons in the self-consistent process to understand its effects on the polarization. Only after this is done will it be significant to inquire about the effects of the assumed $f$ state and of improved functionals. Then one can ask about the effects of the further couplings which must be present as seen from the wealth of magnetic structure data available for this material. Much is yet to be learned from further study of this material.

## ACKNOWLEDGMENTS

[1]H. Kitazawa, T. Suzuki, M. Sera, Z. Oguro, A. Yanase, A. Hasegawa, and T. Kasuya, J. Magn. Magn. Mater. 31-34, 421 (1983).

[2]K. Takegahara, H. Takahashi, A. Yanase, and T. Kasuya, Solid State Commun. 39, 857 (1981).

[3]H. Aoki, G. W. Crabtree, W. Joss, and F. Hullinger, J. Appl. Phys. 57, 3033 (1985).

[4]J. M. Wills, B. R. Cooper, and R. Thayamballi, J. Appl. Phys. 57, 3185 (1985); P. Thayamballi and B. R. Cooper, Phys. Rev. B 31, 5998 (1985).

[5]M. R. Norman and D. D. Koelling, Phys. Rev. B 30, 5530 (1984).

[6]C.-O. Almbladh and A. C. Pedroza, Phys. Rev. A 29, 2322 (1984).

[7]U. von Barth and L. Hedin, J. Phys. C 5, 1629 (1972).

[8]D. D. Koelling and G. O. Arbman, J. Phys. F 5, 2041 (1975); O. K. Andersen, Phys. Rev. B 12, 3060 (1975).

[9]B. N. Harmon and D. D. Koelling, J. Phys. C 7, L210 (1974).

[10]A. H. MacDonald, W. E. Pickett, and D. D. Koelling, J. Phys. C 13, 2675 (1980).

[11]G. Lehman, P. Rennert, M. Taut, and H. Wonn, Phys. Status Solidi 37, 27 (1970); O. Jepsen and O. K. Andersen, Solid State Commun. 9, 1763 (1971); O. Jepsen, thesis, Laboratoriet for Elektrofysik, Danmarks Tekniske Hojskole, 1971; G. Lehman and M. Taut, Phys. Status Solidi B 54, 469 (1972); 57, 815 (1973).

[12]G. O. Arbman and D. D. Koelling, Phys. Scr. 5, 273 (1972).

[13]D. G. Shankland, in Computational Methods in Band Theory, edited by P. M. Marcus, J. Janak, and A. Williams (Plenum, New York, 1971), p. 362; D. D. Koelling and J. H. Wood, J. Comp. Phys. (to be published).

[14]N. Elyashar and D. D. Koelling, Phys. Rev. B 13, 5362 (1976); 15, 3620 (1977).

[15]M. R. Norman and D. D. Koelling, Phys. Rev. B 28, 4357 (1983).

[16]M. R. Norman, H. J. F. Jansen, D. D. Koelling, and A. J. Freeman, Solid State Commun. 52, 739 (1984).

[17]J. Schoenes and W. Reim, J Less-Com. Met. 112, 19 (1985).

[18]L. Hodges, D. R. Stone, and A. V. Gold, Phys. Rev. Lett. 19, 655 (1967).